Atmospheric
Chemistry
and Physics

Supplement of

Spatial variability of air pollutants in a megacity characterized by mobile measurements

Reza Bashiri Khuzestani et al.

Correspondence to: Qi Chen (qichenpku@pku.edu.cn)

Section A. Measurement details

A1. Sampling setup

Sampling inlets were installed at the top front of the vehicle, 3.4 m above ground level (Figure S1). Particles were sampled through a stainless steel cone-shape isokinetic inlet, followed by a cyclone (URG, 2000−30EH) to remove particles over 2.5 μm at a flow rate of 15.9 L min^{-1} and were delivered by an electrolytic polished stainless steel tube (1.905 cm outer diameter for 2 m and 0.64 cm outer diameter for 3 m) with a residence time of less than 6 s. Volatile organic compounds (VOCs) were sampled through a Teflon line (0.64 cm outer diameter) with an in-line Teflon filter. Other gas pollutants were sampled separately through a Teflon line and were delivered to various gas analysers via a glass manifold. An Aerodyne ppotential aerosol mass (PAM) oxidative flow reactor (OFR) was installed above the vehicle, which was bypassed for the ambient measurements. Instruments except the CO analyzer alternated sampling the OFR output (15 min) and the ambient bypass line (5 min) at 4.5 L min^{-1} every 20 min. Complete ambient cycles without OFR switching were conducted around 12-1 p.m. on 14 and 18 November, 2018. A weather station was installed on the top of the vehicle that can measure temperature from -40 to 60 °C and relative humidity from 0 to 100%. All the measurement data were recorded with an industrial personal computer (IPC). A GPS (Goome, GM02F) provided precise latitude and longitude data for spatial analysis as well as calculation of moving speed. Four video cameras installed at the four side of the mobile laboratory provided continuous views of on-road conditions.

A2. Instrument operation, calibration, and data analysis

PTR-QiTOF: VOCs and oxygenated VOCs (OVOCs) were measured by a proton transfer reaction quadrupole interface time-of-flight mass spectrometer (PTR-QiTOF), which ionized a fraction of VOCs in proton-transfer reactions with hydronium ions (H_3O^+) with a time resolution of 2 s. The PTR-QiTOF was operated at 3.8 mbar (E/N = 120 Td) for the drift tube with the temperature of 85 ℃ to reach a sensitivity of 850-4350 ncps ppb^{-1} and mass resolution (~4000 m/Δm) during the mobile measurements. The PTR-QiTOF background at each mass was determined by humidified zero air before the measurements. Aromatics, carbonyls, alcohols, and terpenes were calibrated using gas standards (Spectra Gases, ~1 ppm) at five concentration levels from 0.5 to 20 ppb before and after the whole campaign at a relative humidity of around 50%. For uncalibrated species, the quantification was based on the established transmission curve. The instrument operation and data analysis have been described previously (Huang et al., 2019). The species and the corresponding reaction rate (k) measured by PTR-QiTOF are provided in Table S1. The uncertainty was less than 20% for all of the calibrated species with standards. The range of detection limits (3×signal/noise) for the species was 3-190 ppt with an average of 40 ppt. Huang et al., (2019) found the sampling wall losses of less than 5% for most VOCs and 5-25% for IVOCs under conditions that are similar to our experimental settings. IVOCs were not well characterized in this study. We therefore did not apply any correction factor to the reported VOC concentrations.

TOF-ACSM: The chemical composition of non-refractory PM$_{2.5}$ (i.e., ammonium, nitrate, sulfate, chloride, and organic compounds) was measured by a time-of-flight aerosol chemical speciation monitor (TOF-ACSM) with a capture vaporizer (CV). This instrument was equipped with PM$_{2.5}$ aerodynamic lens and a capture vaporizer. The instrument setup has been described previously by (Zheng et al., 2020). The

instrument has a 40-s time resolution, and the data were processed in Tofware (Tofwerk version 2.5.13). A collection efficiency of 1 was applied as verified by Zheng et al. (2020). Calibrations of ionization efficiency (IE) and relative IE of the instrument followed the standard procedures by using 350 nm pure NH_4NO_3 and $(NH_4)_2SO_4$ before and after the whole campaign (Canagaratna et al., 2007). Calibrations were done before the campaign at 293 K and 1 atm.

Gas analyzers: Various gas analyzers were used to measure CO_2, NO_2, NO, SO_2, O_3, and, CO with detection ranges (precision) of 0-1000 ppm (1%), 0-500 ppb (0.5%), 0-500 ppb (1%), 0-500 ppb (0.5%), 0-20 ppm (0.5%), and 0-10 ppm (1%), respectively. Calibrations using standard gases were conducted before and after the whole campaign.

A3. Source apportionment of organic aerosol by positive matrix factorization (PMF)

PMF analysis was conducted on the organic mass spectra by using the Igor PMF evaluation tool (PET, version 3.00B) follow the same procedure as described by Zheng et al. (2020) for CV-TOF-ACSM. The unit-mass-resolution (UMR) mass spectra for organic aerosol between m/z 12 and 200 are used in the PMF analysis. Seven factors were tested in the PMF runs with various rotational parameter (f_{peak}) values (i.e., -1 to 1, stepped by 0.2) and the seed number of 0. The choice of 6 factors (so called the 5-factor solution to exclude the noise factor) for this study was determined by the ratio of Q to Q_{exp} (i.e., the sum of the squares of the uncertainty-weighted residuals to the expected values) and the time series of the factors comparing to external tracers as well as the variations when passing through the OFR (Figure S1) (Liao et al., 2021).

Table S1 lists the detailed description of the PMF analysis. Figures S2-S5 show the diagnostics of the

PMF analysis and the mass spectra and time series of the solutions. The ratios of Q to Q_{exp} decreased significantly when the factor number (p) increasing from 2 to 5, suggesting that five or more factors were needed to account for the majority of the data variance (Figure S2). The noise factor remains in the solution for various p values greater than 2, which was perhaps caused by the motion on the mobile laboratory during operation. The structure in the residual was significantly reduced by increasing from p of 2 to 6. For p = 6, the primary OA factors showed fragmentation patterns (e.g., C_nH_{2n+1} and C_nH_{2n-1} series for hydrocarbon-like OA (HOA)) and marker fragments (e.g, m/z 55 for cooking-related OA (COA)) that were consistent with CV source profiles of vehicle exhaust and cooking emissions (Figure S3a) (Zheng et al., 2020). These two POA factors were mixed in the solution for p = 5 (Figure S4b). Oxygenated OA (OOA) factors were clearly splitting for p = 7 (Figure S4b). We therefore chose p of 6 as the optimum solution herein. The f_{peak} values did not the ratios of Q to Q_{exp} much but affected the mass spectra of the OA factors. We chose f_{peak} of -0.2 as the selected solution to obtain the mass spectra of the OA factors that were most similar to the source profiles provided by Zheng et al. (2020) for the CV instruments.

For the selected solution, the mass concentrations of the primary factors decreased when passing through the OFR, which was consistent with the induced conversion of POA to SOA under photochemical aging (Figure S3b) (Liao et al., 2021). Under ambient conditions, the mass concentrations of the primary factors sometimes showed high peaks (plumes), which can be explained by transient plumes. Our measurements were on the road and near the vehicle emissions. The 4th Ring Road passes through residential and commercial areas where cooking plumes from restaurants may also affect the on-road air.

The HOA and COA factors might be mixed with other primary OA sources which cannot be resolved in the data collected herein. For example, biomass burning (BBOA) or coal burning (CCOA) were not resolved in this data set. Their contributions to OA were expected to be small because of the stringent emission control in NCP since 2017 (Zheng et al., 2020).

By contrast, the mass concentrations of secondary OA factors increased significantly after photochemical oxidation in the OFR. The mass spectra of these factors also showed elevated m/z 44 that was often used as a marker of oxidative aging. Liao et al (2021) provides detailed descriptions for the PMF results for the OFR data that collected in the same campaign. As shown in Figure S3a, one of the oxygenated OA factors has a prominent m/z 44 in the spectra. We named this one as more-oxidized oxygenated OA (MO-OOA). The other two OOA factors showed significant increased mass in the OFR regardless of the rotation choice. The intensities of m/z 44 was most sensitive to the rotation choice. As shown in Figure S5, the marker fragments remained in the OA factors for various f_{peak} values. The major change was attributed to m/z 44. For positive f_{peak} values, the intensity of m/z 44 was deconvolved to MO-OOA predominantly. Therefore, the mass concentrations of MO-OOA might be biased in the PMF rotations. Zheng et al. (2020) indicated that the OOA factors in the CV spectra show greater mass loadings compared to those obtained by aerosol mass spectrometers with standard vaporizer (SV), which might be explained by the changes of signal-to-noise ratios of ions. Large uncertainties remain in the mass quantification of primary and secondary PMF factors.

References

Canagaratna, M. R., Jayne, J. T., Jimenez, J. L., Allan, J. D., Alfarra, M. R., Zhang, Q., Onasch, T. B., Drewnick, F., Coe, H., Middlebrook, A., Delia, A., Williams, L. R., Trimborn, A. M., Northway, M. J., DeCarlo, P. F., Kolb, C. E., Davidovits, P., and Worsnop, D. R.: Chemical and microphysical characterization of ambient aerosols with the aerodyne aerosol mass spectrometer, Mass Spectrom. Rev., 26, 185-222, https://doi.org/10.1002/mas.20115, 2007.

Huang, G. C., Liu, Y., Shao, M., Li, Y., Chen, Q., Zheng, Y., Wu, Z. J., Liu, Y. C., Wu, Y. S., Hu, M., Li, X., Lu, S. H., Wang, C. J., Liu, J. Y., Zheng, M., and Zhu, T.: Potentially important contribution of gas-phase oxidation of naphthalene and methylnaphthalene to secondary organic aerosol during haze events in Beijing, Environ. Sci. Technol., 53, 1235-1244, https://doi.org/10.1021/acs.est.8b04523, 2019.

Li, B. W., Ho, S. S. H., Xue, Y. G., Huang, Y., Wang, L. Q., Cheng, Y., Dai, W. T., Zhong, H. B., Cao, J. J., and Lee, S. C.: Characterizations of volatile organic compounds (VOCs) from vehicular emissions at roadside environment: The first comprehensive study in Northwestern China, Atmos. Environ., 161, 1-12, https://doi.org/10.1016/j.atmosenv.2017.04.029, 2017.

Li, J., Xie, S. D., Zeng, L. M., Li, L. Y., Li, Y. Q., and Wu, R. R.: Characterization of ambient volatile organic compounds and their sources in Beijing, before, during, and after Asia-Pacific Economic Cooperation China 2014, Atmos. Chem. Phys., 15, 7945-7959, https://doi.org/10.5194/acp-15-7945-2015, 2015.

Li, J., Wu, R. R., Li, Y. Q., Hao, Y. F., Xie, S. D., and Zeng, L. M.: Effects of rigorous emission controls on reducing ambient volatile organic compounds in Beijing, China, Sci. Total Environ., 557, 531-541, https://doi.org/10.1016/j.scitotenv.2016.03.140, 2016.

Li, K., Li, J. L., Wang, W. G., Tong, S. R., Liggio, J., and Ge, M. F.: Evaluating the effectiveness of joint emission control policies on the reduction of ambient VOCs: Implications from observation during the 2014 APEC summit in suburban Beijing, Atmos. Environ., 164, 117-127, https://doi.org/10.1016/j.atmosenv.2017.05.050, 2017.

Li, K., Li, J. L., Tong, S. R., Wang, W. G., Huang, R. J., and Ge, M. F.: Characteristics of wintertime VOCs in suburban and urban Beijing: Concentrations, emission ratios, and festival effects, Atmos. Chem. Phys., 19, 8021-8036, https://doi.org/10.5194/acp-19-8021-2019, 2019.

Li, Y. Q., Li, J., Wu, R. R., and Xie, S. D.: Characterization and source identification of ambient volatile organic compounds (VOCs) in a heavy pollution episode in Beijing, China, in: Air Pollution Xxiv, edited by: Longhurst, J. W. S., Brebbia, C. A., and Barnes, J., WIT Transactions on Ecology and the Environment, Wit Press, Southampton, 249-259, 2016.

Liao, K., Chen, Q., Liu, Y., Li, Y. J., Lambe, A. T., Zhu, T., Huang, R.-J., Zheng, Y., Cheng, X., Miao, R., Huang, G., Khuzestani, R. B., and Jia, T.: Secondary organic aerosol formation of fleet vehicle

emissions in China: Potential seasonality of spatial distributions, Environ. Sci. Technol., https://doi.org/10.1021/acs.est.0c08591, 2021.

Yang, Y., Ji, D. S., Sun, J., Wang, Y. H., Yao, D., Zhao, S., Yu, X. N., Zeng, L. M., Zhang, R. J., Zhang, H., Wang, Y. H., and Wang, Y. S.: Ambient volatile organic compounds in a suburban site between Beijing and Tianjin: Concentration levels, source apportionment and health risk assessment, Sci. Total Environ., 695, 13, https://doi.org/10.1016/j.scitotenv.2019.133889, 2019.

Zheng, Y., Cheng, X., Liao, K. R., Li, Y. W., Li, Y. J., Hu, W. W., Liu, Y., Zhu, T., Chen, S. Y., Zeng, L. M., Worsnop, D., Chen, Q., and Huang, R. J.: Characterization of anthropogenic organic aerosols by TOF-ACSM with the new capture vaporizer, Atmos. Meas. Tech., 13, 2457-2472, https://doi.org/10.5194/amt-13-2457-2020, 2020.

Table S1. Detailed descriptions of the PMF solutions.

Factor Number (p)	Fpeak	Seed	Q/Q_{exp}	Solution Description
1	0	0	4.97	Too few factors and large residuals
2	0	0	3.78	Q/Q_{exp} decreases by 24% of the maximum Q. There still exist large residuals at time periods and key m/z. One of the two factors is perhaps the POA-OOA mixture while the other is the MO-OOA type.
3	0	0	2.70	Q/Q_{exp} decreases by additional 22% of the maximum Q. There still exist large residuals at time periods and key m/z. The POA-OOA mixture and MO-OOA remains while a noise factor appears.
4	0	0	2.12	Q/Q_{exp} decreases by additional 11% of the maximum Q. There still exist large residuals at time periods and key m/z. The noise factor remains. One factor is POA-like and the other two are OOAs (MO-OOA and LO-OOA).
5	0	0	1.77	Q/Q_{exp} still decreases significantly by additional 6% of the maximum Q. The noise factor remains. The four factors include one POA-like and three OOAs (MO-OOA, and two LO-OOAs) (Figure S4a).
6 (5-factor solution as the optimum choice herein)	-0.2	0	1.68	Q/Q_{exp} decreases by additional 2% of the maximum Q. The noise factor remains. Two POA factors are resolved (one HOA-like and one COA-like). The other three OOAs remain including one MO-OOA and two LO-OOAs (Figure S3a). In particular, when passing through the OFR, the mass concentrations of OOA factors all increased whereas those of HOA and COA decreased because of photochemical aging, supporting the identification of the POA and SOA factors (Liao et al., 2021).
7	0	0	1.63	Q/Q_{exp} decreases by additional 1% of the maximum Q. The noise factor remains. The other six factors include four OOAs and two POAs (Figure S4b). OOAs clearly split.

Table S2. The average concentrations of the 52 VOC species measured in this study compared with literature. These species are tentatively categorized into three groups including hydrocarbons (Group 1), aldehydes and ketones (Group 2), and acids and anhydrides (Group 3).

Formula		Assigned Name	m/z	K_{PTR}	Category /Group	Mean ±sd (non-haze)	Mean ±sd (haze)	Urban[*]	Suburb[*]
Calibrated species	$(CH_3OH)H^+$	Methanol	33.033	2.22	n/a	16.82±14.81	44.69±15.96	11.77-51.76	3.4-5.6
	$(C_2H_2O)H^+$	Ketenes	43.018	2.21	2	2.12±1.84	5.42±1.42		
	$(C_2H_4O)H^+$	Acetaldehyde	45.033	3.36	2	2.72±2.00	6.07±1.63	1.88-15.81	0.83-1.23
	$(C_2H_6O)H^+$	Ethanol	47.049	2.18	n/a	25.35±32.19	98.28±32.17		
	$(C_3H_4O)H^+$	Acrolein; MTBE	57.033	3.35	2	0.30±0.27	0.60±0.14		
	$(C_3H_6O)H^+$	Acetone + propanal	59.049	3	2	1.20±1.18	4.67±0.97	2.48-7.92	1.59-3.42
	$(C_5H_8)H^+$	Isoprene; fragmentation of 2- methyl-3-buten-2-ol (MBO); fragmentation of cyclohexanes	69.07	1.94	1	0.38±0.35	0.76±0.20		
	$(C_4H_6O)H^+$	Methyl vinyl ketone + methacrolein; crotonaldehyde; ISOPOOH	71.049	3.83	2	0.16±0.14	0.36±0.09	0.28-0.42	0.13-0.22
	$(C_4H_8O)H^+$	Methyl ethyl ketone + butanals	73.065	3.48	2	1.56±2.45	1.51±0.44	0.86-2.53	0.38-0.81
	$(C_6H_6)H^+$	Benzene	79.054	1.97	1	0. 78±0.59	2.90±0.73	1.2-4.3	0.91-1.9
	$(C_5H_{10}O)H^+$	Pentanone + pentanal; 2-methyl-3-buten-2-ol (MBO)	87.08	3.35	2	0.05±0.04	0.14±0.05		
	$(C_4H_8O_2)H^+$	Ethyl acetate; butyric acid	89.06	4.3	3	0.06±0.06	0.22±0.06		
	$(C_7H_8)H^+$	Toluene	93.07	2.12	1	1.00±0.94	3.09±0.89	1.51-6.11	0.73-3.31
	$(C_6H_{12}O)H^+$	Methyl isobutyl ketone; hexanal	101.096	2.28	2	0.04±0.04	0.09±0.06		
	$(C_8H_8)H^+$	Styrene	105.07	2.33	1	1.53±2.02	5.82±3.21	0.21-0.62	0.1-0.14
	$(C_8H_{10})H^+$	Xylenes; C_8 aromatics	107.086	2.29	1	0.84±1.03	2.59±1.14	1.1-7.35	0.71-1.17
	$(C_9H_{12})H^+$	Trimethylbenzenes; C_9 aromatics	121.1	2.47	1	0.27±0.24	0.59±0.25	0.31-1.35	0.21-1.02
	$(C_{10}H_{16})H^+$	Monoterpenes	137.132	2.44	1	0.07±0.09	0.18±0.10	0.06-0.39	0.04-0.27

10

	Ion	Description							
Uncalibration species with known K_{PTR}	$(C_3H_4)H^+$	Fragmentation from isoprene or other hydrocarbons	41.039	1.58	1	1.02 ±0.47	5.31 ±2.04		
	$(C_3H_6)H^+$	Propene; fragmentation from hydrocarbons and propanols	43.054	1.58	1	0.15 ±0.05	0.71 ±0.21		
	$(CH_2O_2)H^+$	Formic acid	47.013	2.02	3	0.74 ±1.11	3.15 ±2.26	2.39-4.39	2.73-3.02
	$(C_4H_8)H^+$	Butenes; fragments from butanol or other hydrocarbons	57.06	1.76	1	0.70 ±1.02	2.55 ±1.03		
	$(C_2H_4O_2)H^+$	Acetic acid; glycolaldehyde; fragmentation of ethyl acetate	61.028	2.27	3	2.02 ±1.67	5.76 ±1.23	4.0-4.5	2.31-4.06
	$(C_2H_6S)H^+$	Dimethyl sulfide	63.023	2	n/a	0.04 ±0.03	0.20 ±0.11		
	$(C_4H_4O)H^+$	Furan	69.033	1.78	2	0.06 ±0.06	0.13 ±0.05		
	$(C_3H_4O_2)H^+$	Methylglyoxal; acrylic acid	73.028	2.67	2	0.12 ±0.11	0.21 ±0.06		
	$(C_3H_6O_2)H^+$	Hydroxyacetone; propanoic acid	75.044	2.41	2	0.30 ±0.31	1.06 ±0.25		
	$(C_6H_{10})H^+$	Hexyne; methylcyclopentane	83.085	2.16	1	0.13 ±0.14	0.33 ±0.10		
	$(C_4H_6O_2)H^+$	Butanedione; methacrylic acid	87.044	4.51	3	0.06 ±0.06	0.15 ±0.05		
	$(C_6H_6O)H^+$	Phenol	95.049	2.52	2	0.01 ±0.02	0.12 ±0.09		
	$(C_5H_4O_2)H^+$	Furfural	97.028	4.83	2	0.10 ±0.10	0.11 ±0.04		
	$(C_7H_{12})H^+$	Cycloheptene; methylcyclohexane	97.1	2.09	1	0.07 ±0.07	0.16 ±0.06		
	$(C_5H_8O_2)H^+$	Glutaraldehyde; pentanediones, pentenoic acid	101.061	3.9	3	0.05 ±0.04	0.12 ±0.04		
	$(C_7H_6O)H^+$	Benzaldehyde	107.049	4.12	2	0.02 ±0.04	0.17 ±0.06		
	$(C_7H_{14}O)H^+$	Heptanal; heptanone; methyl hexanone	115.11	3.14	2	0.01 ±0.01	0.02 ±0.01		
	$(C_8H_8O)H^+$	Tolualdehyde; methylbenzaldehyde	121.063	3.84	2	0.01 ±0.01	0.06 ±0.03		
	$(C_7H_6O_2)H^+$	Benzoic acid; hydroxybenzaldehyde	123.044	3.02	3	0.02 ±0.04	0.04 ±0.03		
	$(C_{10}H_8)H^+$	Naphthalene	129.07	2.59	1	0.06 ±0.06	0.13 ±0.08		

	$(C_2H_4O_3)H^+$	PAN; glycolic acid; peracetic acid	77.023	2	3	0.03 ±0.04	0.07 ±0.09
	$(C_5H_6O)H^+$	Methyl furan	83.049	2	2	0.06 ±0.05	0.14 ±0.05
	$(C_3H_4O_3)H^+$	Pyruvic acid; ethylene carbonate	89.024	2	3	0.05 ±0.09	0.13 ±0.08
	$(C_6H_8O)H^+$	Dimethyl furans; cyclohexenone; methyl cyclopentenone	97.064	2	2	0.03 ±0.03	0.10 ±0.04
Uncalibration species with unknown K_{PTR}	$(C_4H_4O_3)H^+$	Succinic anhydride; hydroxyfuranone; fumaraldehydic acid	101.023	2	3	0.07 ±0.12	0.16 ±0.10
	$(C_5H_4O_3)H^+$	Furoic acid; citraconic anhydride	113.024	2	3	0.11 ±0.14	0.12 ±0.10
	$(C_6H_8O_2)H^+$	Sorbic acid; hexadienic acid	113.056	2	3	0.04 ±0.05	0.12 ±0.06
	$(C_7H_{12}O)H^+$	Methylcyclohexanones; heptenone; heptenal; dimethylpentenone	113.096	2	2	0.01 ±0.01	0.04 ±0.02
	$(C_5H_6O_3)H^+$	Glutaric anhydride; pentenoic acid	115.038	2	3	0.02 ±0.03	0.04 ±0.03
	$(C_6H_{10}O_2)H^+$	Hexenoic acid; ethyl butenoate; hexanedione	115.075	2	3	0.02 ±0.02	0.05 ±0.05
	$(C_4H_4O_4)H^+$	Fumaric acid; formyl pyruvate	117.018	2	3	0.01 ±0.01	0.04 ±0.07
	$(C_5H_8O_3)H^+$	Levulinic acid; methyloxobutanoic acid;	117.057	2	3	0.01 ±0.01	0.01 ±0.02
	$(C_6H_{12}O_2)H^+$	C_6 acids (acetate)	117.09	2	3	below detection limit	0.02 ±0.03
	$(C_8H_{10}O)H^+$	C_2 phenols	123.08	2	2	below detection limit	0.01 ±0.01

[*](Li et al., 2019; B. W. Li et al., 2017; Li et al., 2015; J. Li et al., 2016; K. Li et al., 2017; Yang et al., 2019; Y. Q. Li et al., 2016)

Table S3. The mean concentrations of air pollutants measured by the mobile laboratory during the non-haze and haze periods (9 a.m. to 4 p.m.). The unit for NR-PM$_{2.5}$ and its chemical components is μg m^{-3}. The unit for CO is ppmv and for other gaseous pollutants is ppbv.

Air pollutants		Non-haze		Haze
		Weekday	Weekend	
NR-PM$_{2.5}$	OA	17.0±7.6	15.4±6.7	46.4±10.4
	Nitrate	14.3±5.9	9.5±6.1	54.4±7.7
	Sulfate	2.0±1.3	1.2±0.3	28.8±7.2
	Ammonium	4.8±2.5	3.3±2.6	27.2±4.5
	Chloride	0.3±0.3	0.2±0.2	2.0±1.0
	Total NR-PM$_{2.5}$	39.3±150	29.6±12.8	160.2±21.6
Detected VOCs and OVOCs	Σ Hydrocarbons	9.1±7.5	8.7±4.6	20.0±4.0
	Σ (Aldehyde & Ketones)	9.4±4.1	8.5±2.8	21.6±3.2
	Σ (Acids & Anhydrides)	6.6±2.4	5.6±1.3	10.6±1.2
	Total	25.2±12.2	22.6±7.7	52.2±6.7
Others	SO$_2$	4.6±1.2	6.5±0.9	5.3±0.8
	CO	1.6±0.6	0.8±0.2	3.0±0.6
	NO	186.4±77.1	105.9±23.1	174.2±51.7
	NO$_2$	107.6±40.6	84.4±8.6	69.7±26.5
	O$_3$	10.3±3.4	11.3±2.5	13.8±2.9

Table S4. The coefficients of variation (CV) values for the mean concentrations of air pollutants measured on the 4th Ring Road during the non-haze and the haze days. Data covered from 9 a.m. to 4 p.m. during the measurement period.

Air pollutants		CV values	
		Non-haze	Haze
NR-PM$_{2.5}$	OA	0.38	0.17
	Nitrate	0.59	0.13
	Sulfate	0.54	0.20
	Ammonium	0.42	0.14
	Chloride	0.84	0.35
	Total NR-PM$_{2.5}$	0.37	0.14
Detected VOCs and OVOCs	Σ Hydrocarbons	0.72	0.20
	Σ (Aldehyde & Ketones)	0.40	0.15
	Σ (Acids & Anhydrides)	0.39	0.11
	Total	0.40	0.13
Others	SO$_2$	0.16	0.25
	CO	0.23	0.20
	NO	0.20	0.22
	NO$_2$	0.24	0.26
	O$_3$	0.19	0.21
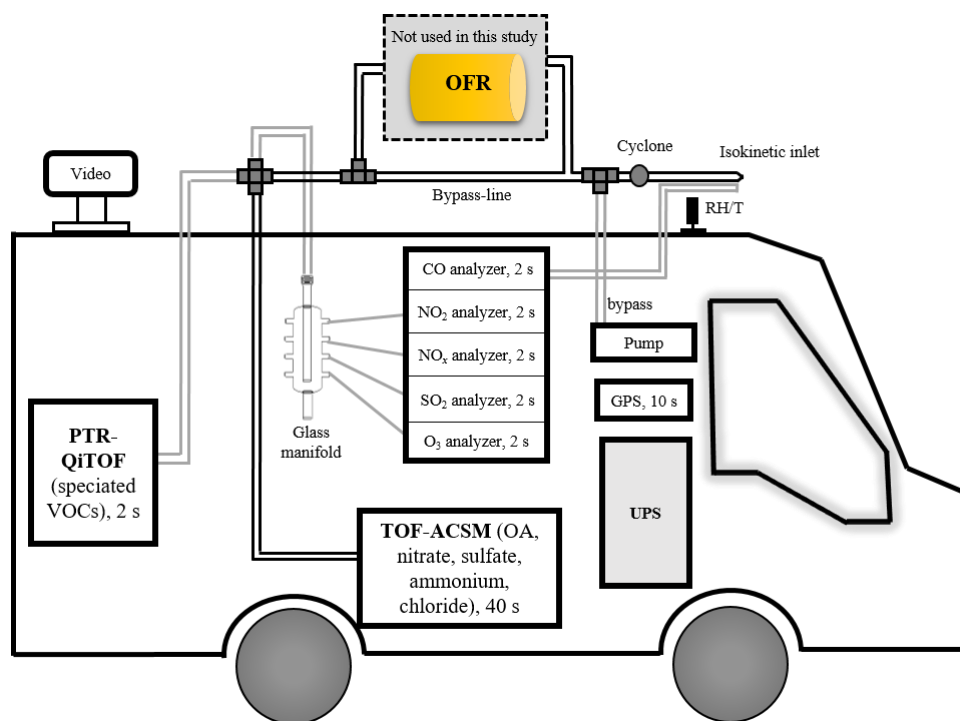
Figure S1. Schematic of the PKU mobile laboratory. The black and grey lines represent stainless steel and Teflon tubes, respectively. Temporal resolutions for each instrument are shown with a unit of second. The data when the sampling air passed through the oxidative flow reactor (OFR) were not included in the analysis herein.
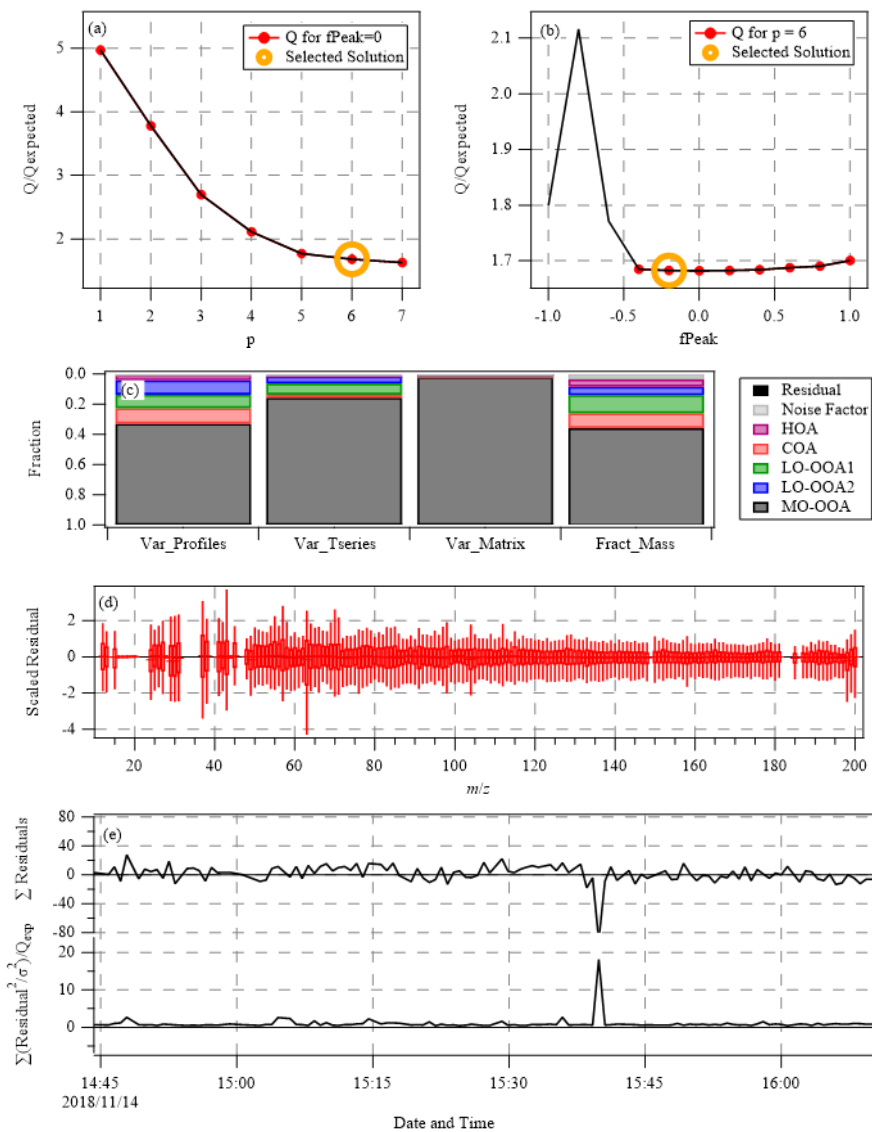
Figure S2. PMF diagnostics for (a) Q/Q_{exp} for different factor numbers, (b) Q/Q_{exp} for different f_{peak} values, (c) variance, (d) scaled residuals for all m/z, and (e) residuals. Residuals were zoomed in for the haze-day data on 14 November 2018.
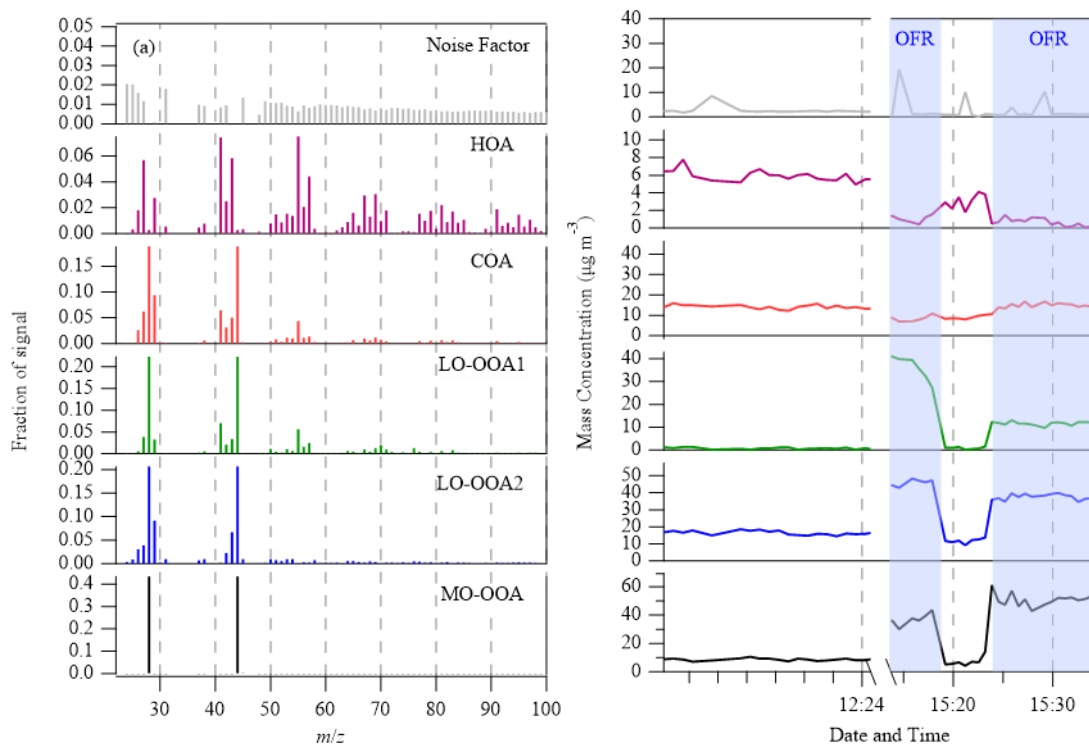
Figure S3. (a) Mass spectra and (b) time series of the OA factors identified by the PMF analysis for the "5-factor" solution ($p = 6$, $f_{peak} = -0.2$). The time series were zoomed in for the haze-day data on 14 November 2018. OFR data were not used in this study.
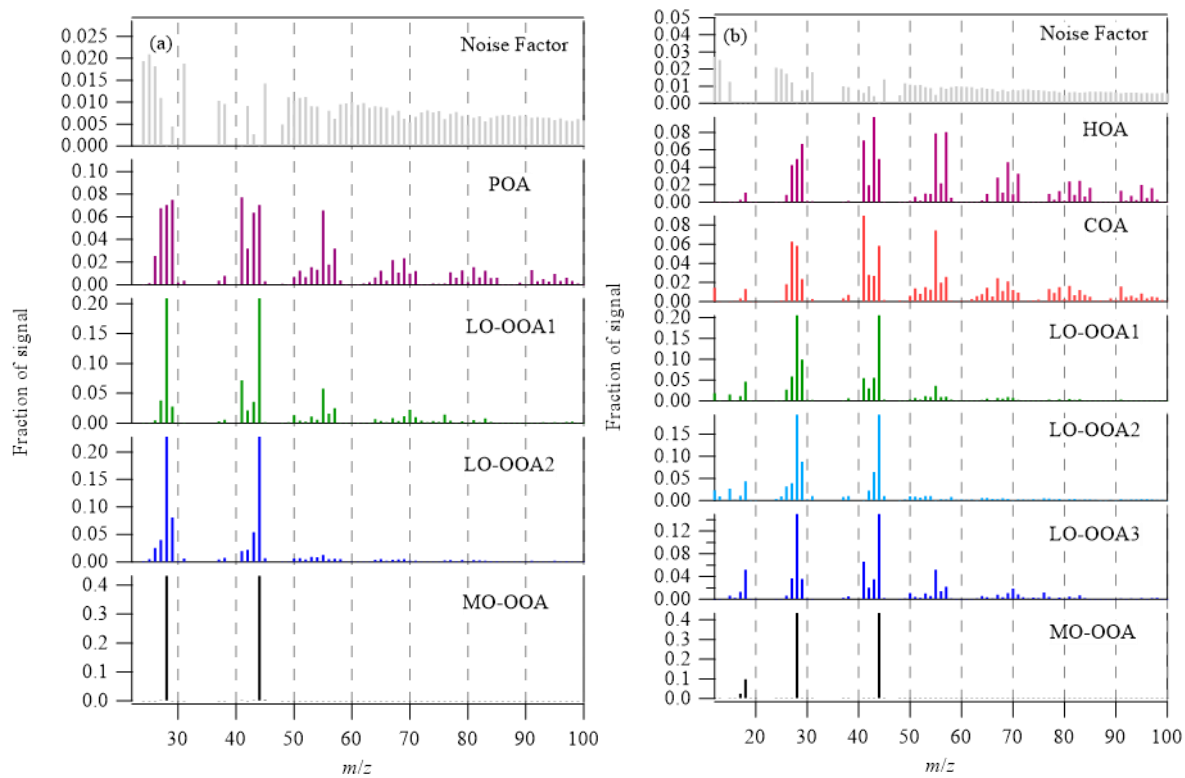
Figure S4. Mass spectra of the OA factors identified by the PMF analysis for (a) the "4-factor" solution

$(p = 5, f_{peak} = -0.2)$ and (b) the "6-factor" solution $(p = 7, f_{peak} = -0.2)$.
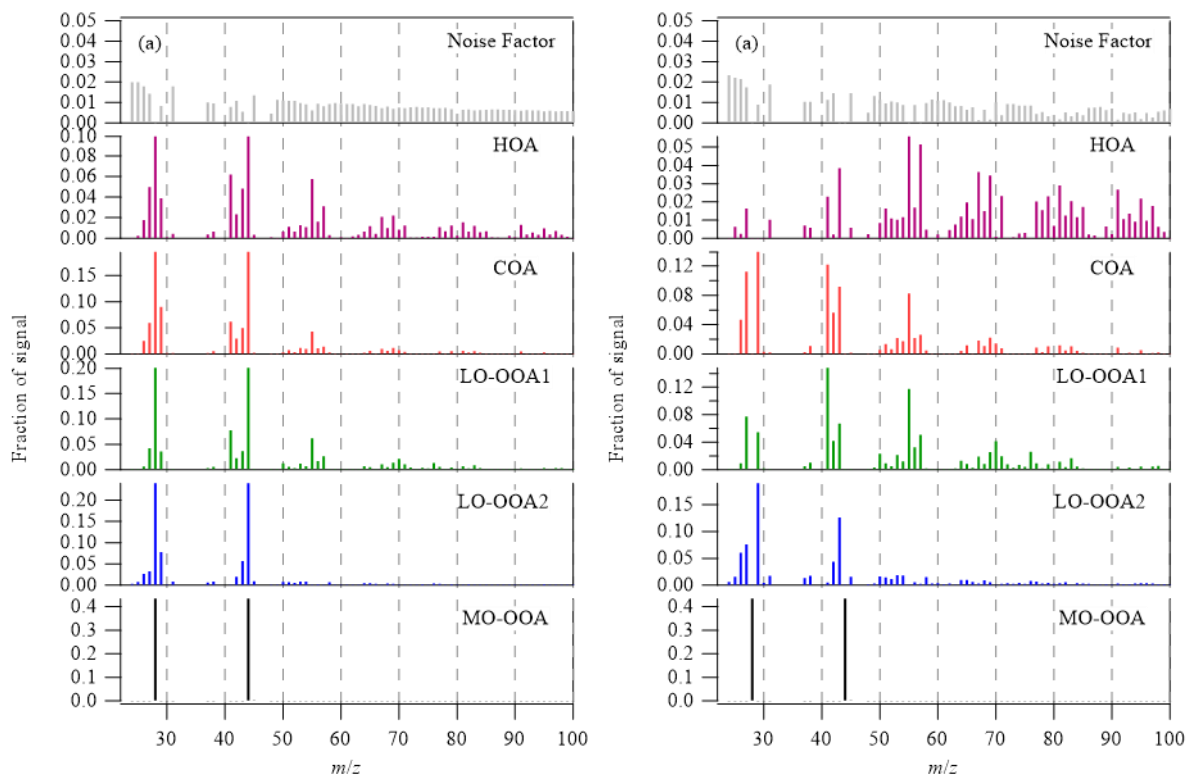
Figure S5. Mass spectra of the OA factors identified by the PMF analysis for the "5-factor" solution (p = 6) for (a) $f_{peak} = -0.4$ and (b) $f_{peak} = 0.4$.
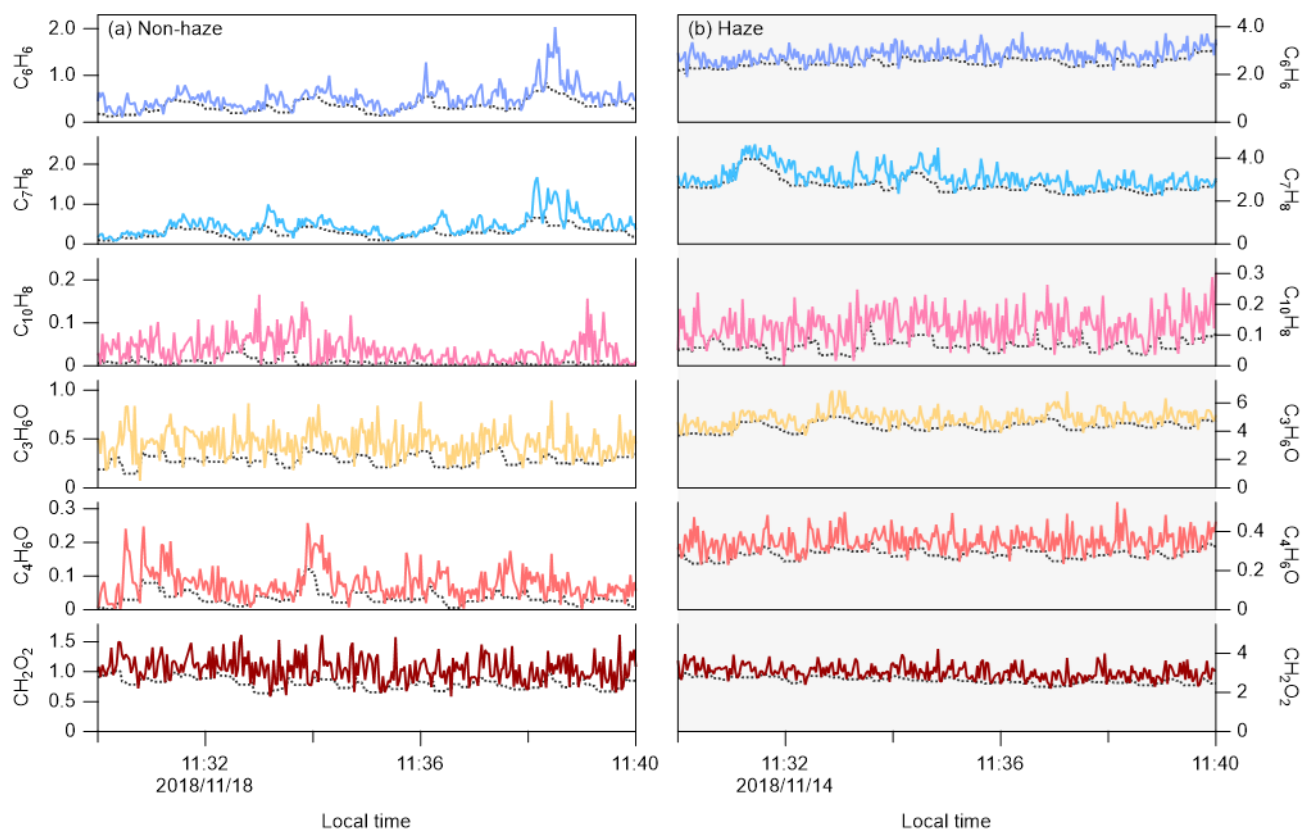
Figure S6. Time series of the mixing ratios of selected VOC and OVOC species for typical runs. Data are shown for the complete cycles on the 4th Ring Road during (a) the clean day on 18 November 2018 and (b) the haze day on 14 November 2018. Dashed lines show the calculated baselines by the moving average method.
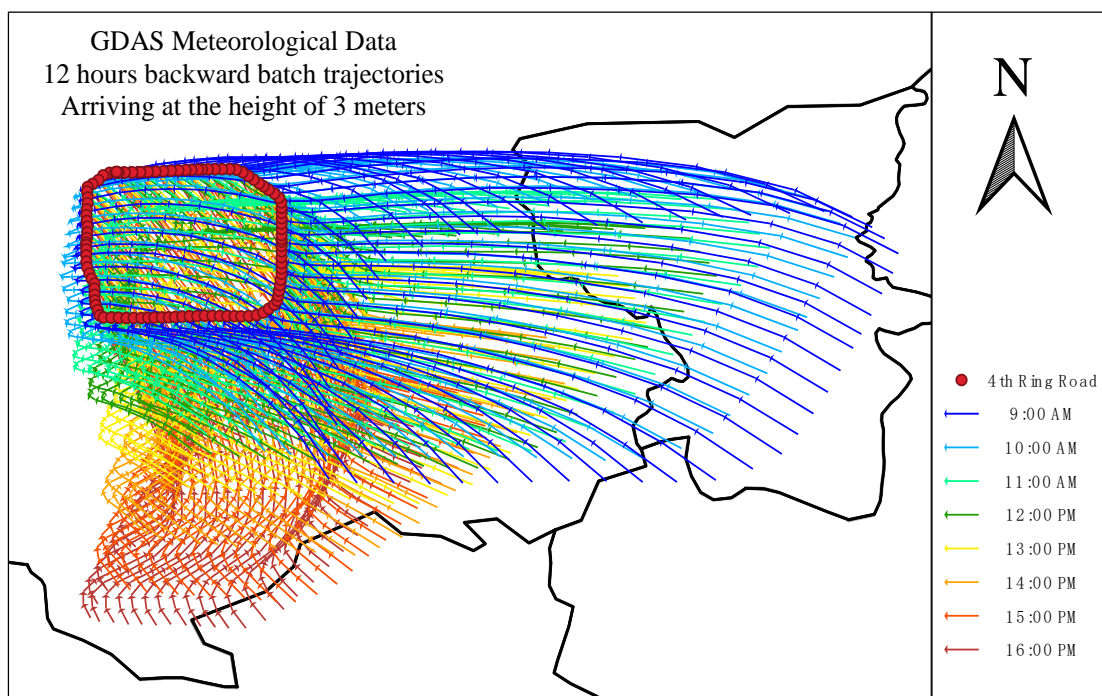
Figure S7. The 12-hour backward trajectories arriving at the height of 3 m of the 4th Ring Road in Beijing during the haze day on 14 November 2018. The start time was 9:00 a.m. and repeated every 1 hours until 4:00 p.m. local time.
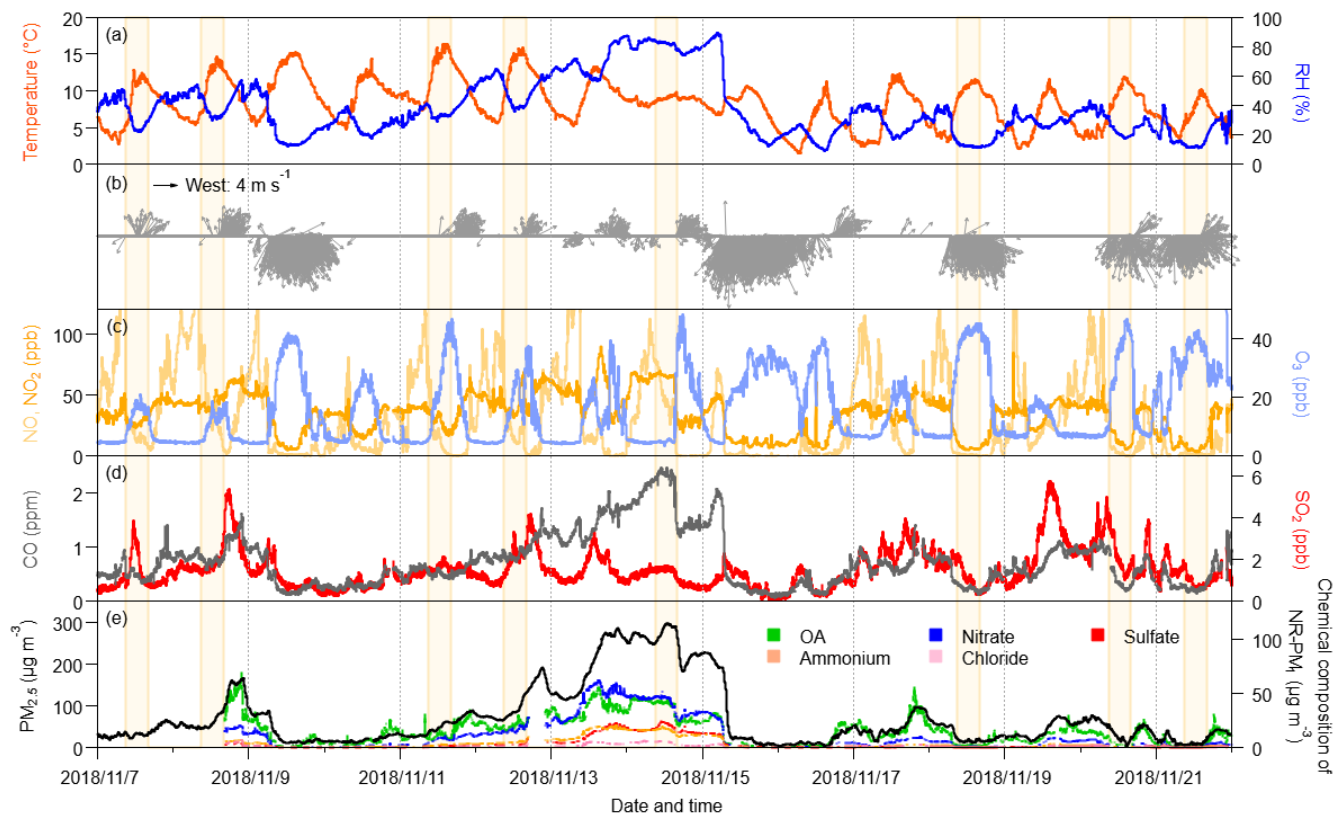
Figure S8. Time series of (a) temperature and relative humidity (RH), (b) wind speed (WS) and wind direction (WD), (c) NO, NO_2, and O_3, (d) CO and SO_2, (e) $PM_{2.5}$ and the chemical composition of NR-PM_1 measured at the PKU campus roof station during the mobile campaign. The yellow-shaded areas represent the periods of mobile measurements.
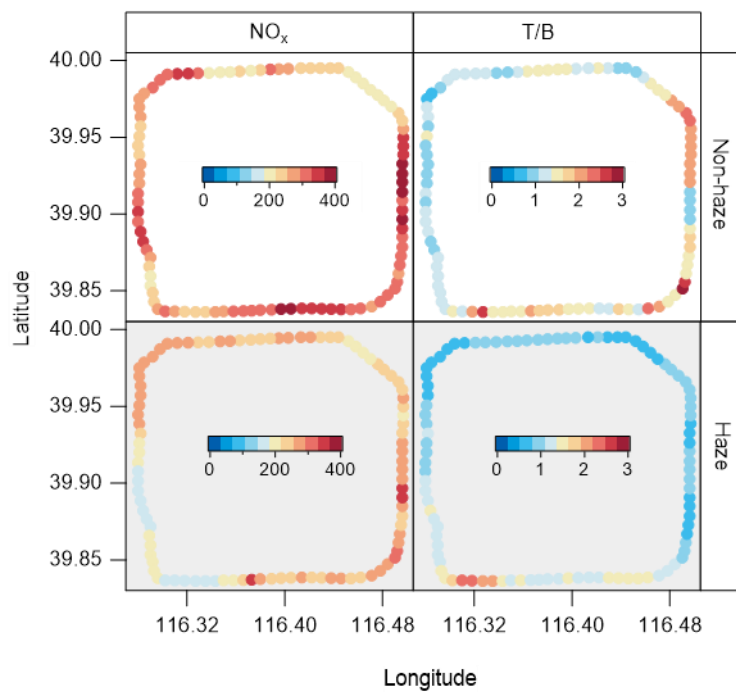
Figure S9. Spatial distributions of NO_x mean mixing ratios and toluene-to-benzene (T/B) ratio measured on the 4th Ring Road in Beijing. Data covered from 9 a.m. to 4 p.m. during the measurement period.
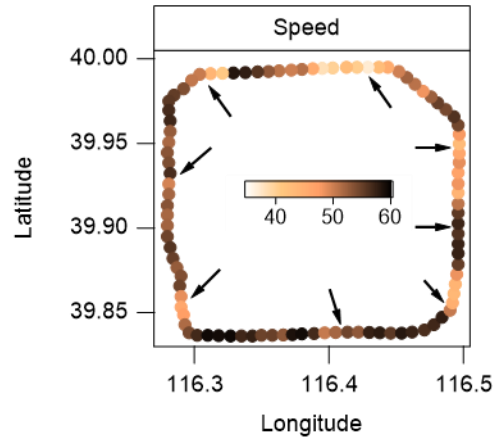
Figure S10. Spatial distributions of the mean driving speed (Unit: km h^{-1}) of the mobile laboratory on the 4th Ring Road in Beijing during the measurement period. Arrows marked the places where HOA shows concentration hotspots. The driving speed was affected by the real-time traffic volume.
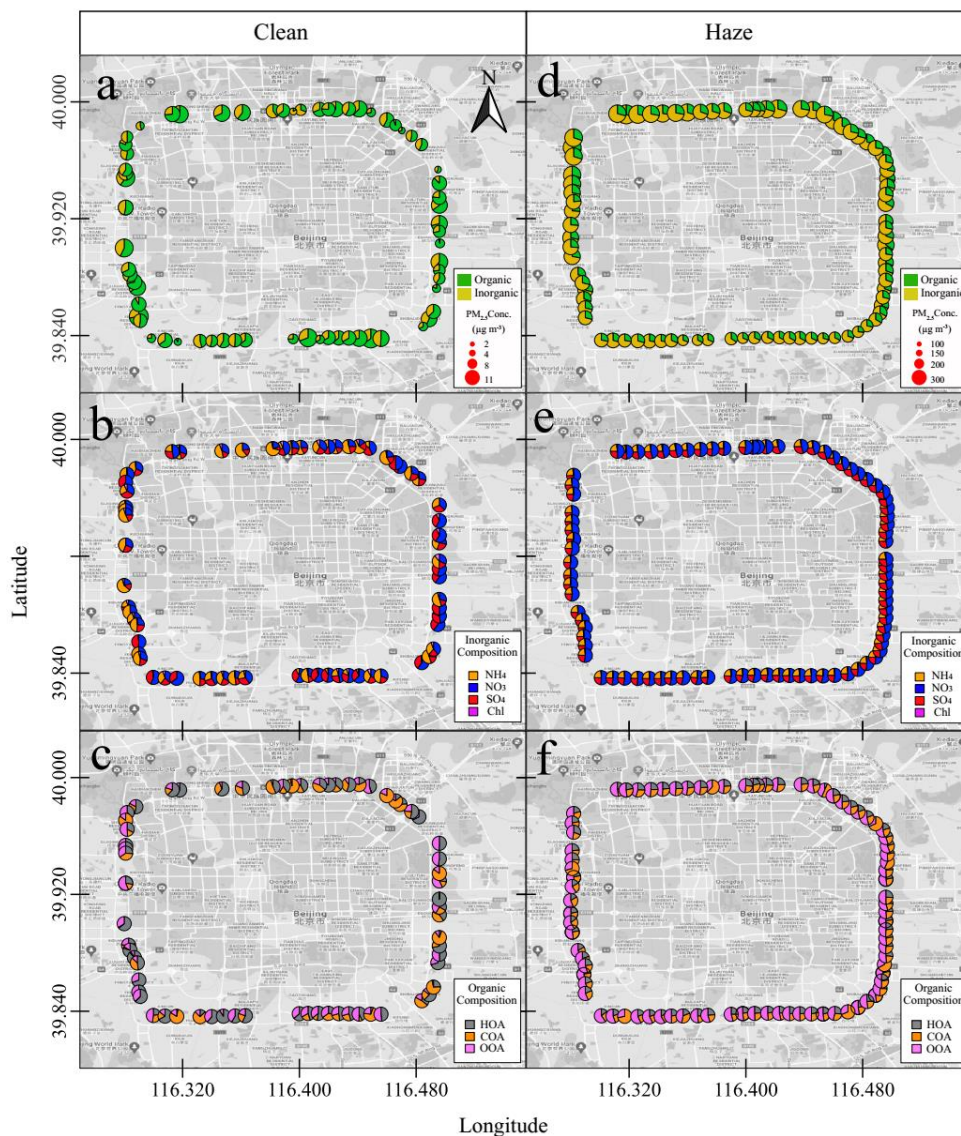
Figure S11. Spatial distribution of (a, d) the mass concentration ($\mu g\ m^{-3}$), (b, e) the inorganic composition, and (c, f) the organic composition of NR-PM$_{2.5}$ measured during the noon cycles from ~11:00 AM to ~12:30 PM for the clean day on 18 November 2018 and the haze day on 14 November 2018 (source: © Google Maps 2020). The size of the pies for inorganic and organic composition is the same and does not correspond to the mass concentrations of components. The organic composition is obtained from the PMF analysis, in which OOA represents the sum of the three OOA factors.
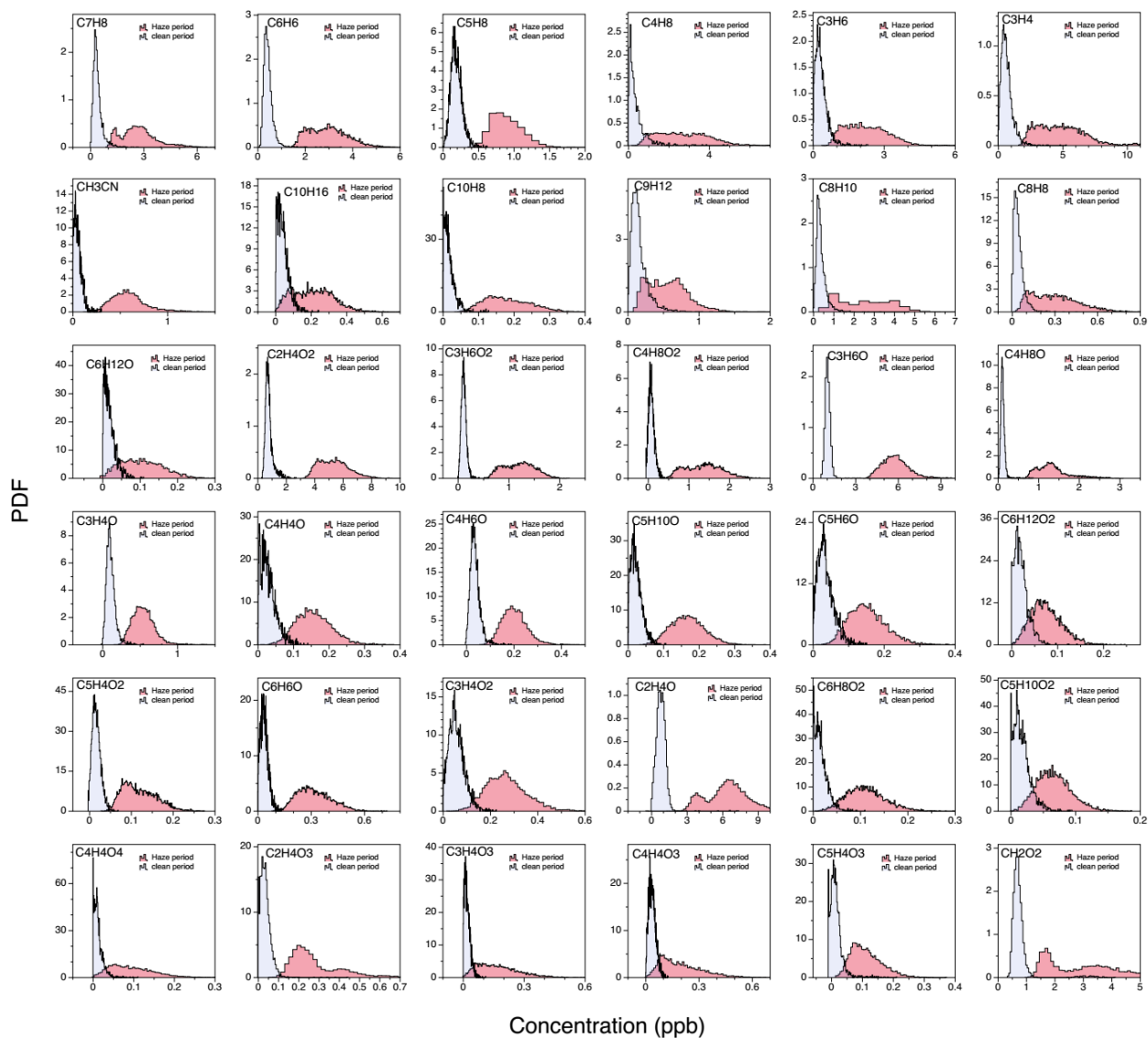
Figure S12. Probability distribution function (PDF) histograms of the mixing ratios of the main VOCs and OVOCs (36 species in total) measured during the clean day on 18 November 2018 and the haze day on 14 November 2018. Data covered from 9 a.m. to 4 p.m.
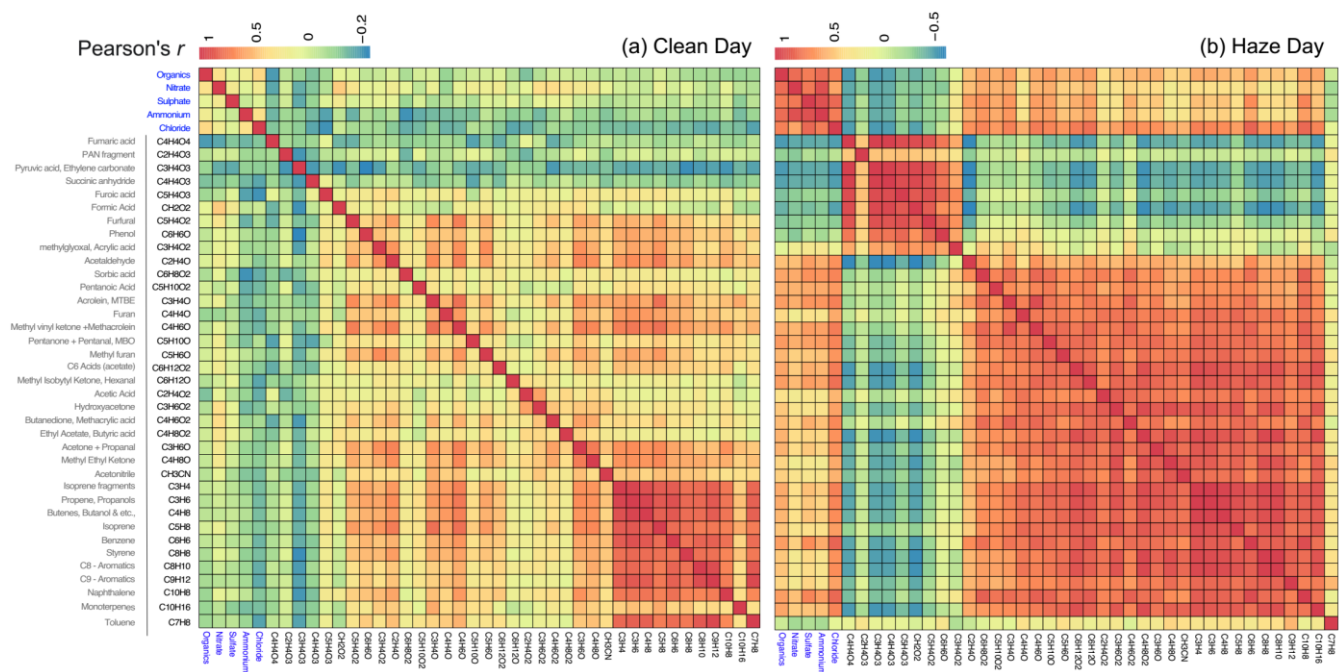
Figure S13. Correlation heatmaps for the concentrations of the main VOCs and OVOCs as well as NR-PM$_{2.5}$ components measured during (a) the clean day on 18 November 2018 and (b) the haze day on 14 November 2018.
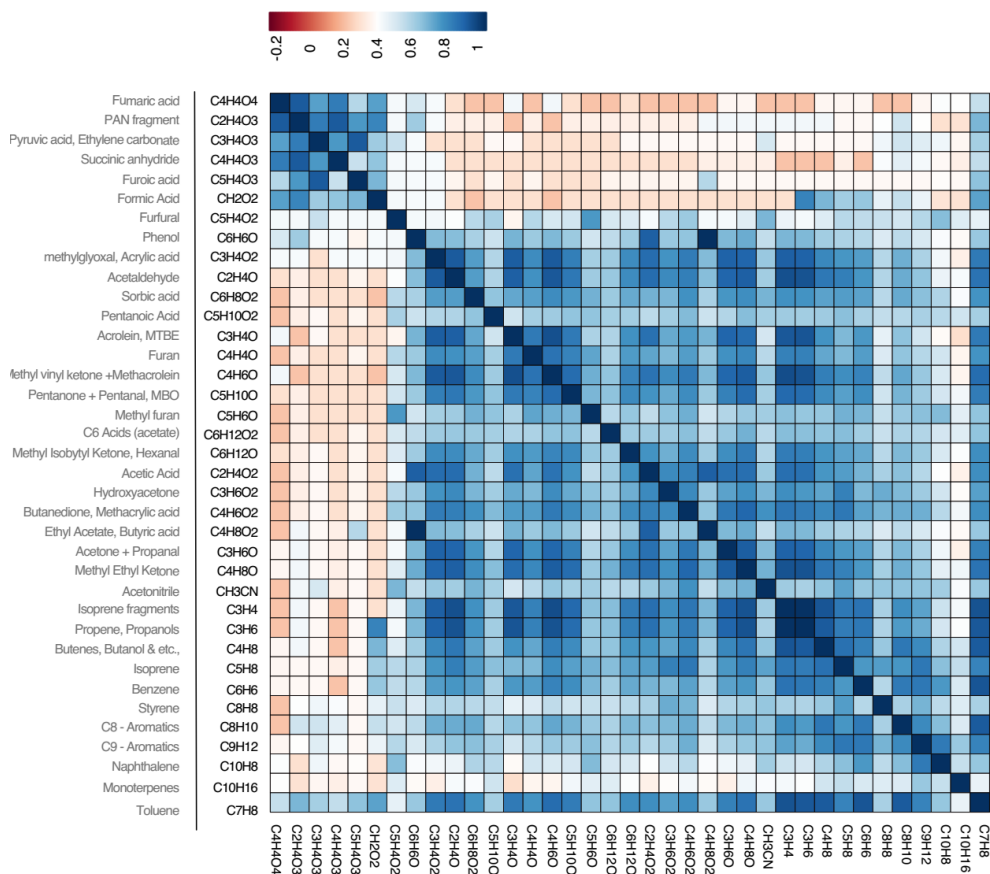
Figure S14. Correlation heatmap for the concentrations of the main VOCs and OVOCs measured during the haze day on 21 January 2021.